coatings

MDPI

Article

Stress Analysis in Tungsten Alloys Modified with Plasma Flows and Irradiated with Helium Ions

Azamat Ryskulov [1,*], Vitaliy Shymanski [2], Bauyrzhan Amanzhulov [1,3,*], Igor Ivanov [1,4], Vladimir Uglov [2], Valiantsin Astashynski [5], Mikhail Koloberdin [1], Anton Kuzmitski [5] and Alisher Kurakhmedov [1,3]

1 Institute of Nuclear Physics, Almaty 050032, Kazakhstan; igor.ivanov.inp@gmail.com (I.I.); kurahmedov.alisher@gmail.com (A.K.)
2 Department of Solid State Physics and Nanotechnologies, Belarusian State University, 220030 Minsk, Belarus; shymanskiv@mail.ru (V.S.); uglov@bsu.by (V.U.)
3 Physical-Technical Faculty, L.N. Gumilyov Eurasian National University, Astana 010008, Kazakhstan
4 Engineering Profile Laboratory, L.N. Gumilyov Eurasian National University, Astana 010008, Kazakhstan
5 A.V. Luikov Heat and Mass Transfer Institute of National Academy of Science of Belarus, 220072 Minsk, Belarus; ast@hmti.ac.by (V.A.)
* Correspondence: ryskulov_nbd@mail.ru (A.R.); amanzholovb96@gmail.com (B.A.)

Abstract: As the development of nuclear fusion depends on plasma-facing materials, new methods for improving the radiation resistance of tungsten are being created and tested. This paper presents the results of studying the structure, surface morphology, phase composition, and residual internal stresses in tungsten alloys modified by plasma flows and irradiated with helium ions with an energy of 40 keV and doses of (1–3) $\times$ 10^{17} cm^{-2}. It is shown that the effect of compression plasma flows on tungsten leads to the modification of its grain structure in the near-surface layer, forming dispersed cells of 220–320 nm in size due to high-speed crystallization. The results of measuring the lattice parameters and internal stresses in irradiated tungsten alloys showed that the near-surface layer accumulates radiation defects, creating internal stresses, the relaxation of which leads to local destruction of the surface. Preliminary plasma treatment creates an increased density of intergranular boundaries, which serve as sinks for radiation defects and increase the radiation resistance of tungsten alloys.

Keywords: tungsten; tungsten–copper alloy; tungsten–zirconium alloy; compression plasma flows; helium ions; ion irradiation; radiation effects; blistering; stress; X-ray diffraction

Academic Editor: Vincent Ji

Received: 13 January 2025
Revised: 30 January 2025
Accepted: 5 February 2025
Published: 7 February 2025

Citation: Ryskulov, A.; Shymanski, V.; Amanzhulov, B.; Ivanov, I.; Uglov, V.; Astashynski, V.; Koloberdin, M.; Kuzmitski, A.; Kurakhmedov, A. Stress Analysis in Tungsten Alloys Modified with Plasma Flows and Irradiated with Helium Ions. *Coatings* **2025**, *15*, 198. https://doi.org/10.3390/coatings15020198

1. Introduction

Currently, methods of modifying the surface of metals and alloys using pulsed plasma flow [1,2], charged particle beams [3,4], and laser radiation [5,6] are widely used. Most of these methods are based on the transfer of high energy density to the surface layer of the material in a relatively short period, estimated from tens of nanoseconds to hundreds of microseconds. The advantage of such methods over traditional thermal, chemical–thermal, and deformation methods is the transformation of the structural-phase state of a thin surface layer, which, as a rule, performs the functional load of the material while maintaining the volumetric properties of the entire product. The most interesting are the exposure modes that allow heating of the surface layer above the melting point and, due to the pulsed energy supply, provide conditions for high-speed quenching from the molten state. The results of modifying the surface layer are usually the creation of a dispersed grain structure [7] and the formation of new or secondary phases [8,9], which together can positively affect the mechanical performance and radiation resistance of materials.

Several recent studies show that the combination of the above-described pulsed high-energy impact on materials with the preliminary formation of additional metal layers on their surface in the form of thin coatings allows alloying of the near-surface layer with elements of this coating [10–12]. A distinctive feature of this approach to alloying is, firstly, its implementation in the liquid phase and, secondly, its occurrence in nonequilibrium conditions. Indeed, the high-speed nature of the input of thermal energy and crystallization indicates the nonequilibrium nature of processes that can increase the solubility limits of elements, form supersaturated solid solutions [10], and produce nanoscale precipitates in the matrix. The liquid-phase alloying mechanism increases the rate of diffusion mass transfer and can implement a new, additional mass transfer mechanism associated with liquid-phase mixing due to hydrodynamic flows. The latter feature of this alloying approach ensures uniform distribution of the alloy components and makes the formed structure homogeneous. However, to implement the liquid-phase alloying process, sufficient duration of the existence of the liquid state on the surface of the unmelted substrate is required, and for refractory materials, this condition is supplemented by the need for high energy density imparted to the material. Such a combination of high pulse duration and high energy density has been implemented in sources of high-current, high-intensity electron beams [13] and in plasma flows generated by quasi-stationary plasma accelerators [14].

The works [15–17] showed that using compression plasma flows allows modifying the surface layers of such practically important metals and alloys as titanium and aluminum alloys, steels, and silicon wafers. From a practical point of view, plasma treatment of the above materials allowed for a significant increase in mechanical parameters and surface wear resistance. However, the radiation resistance of the formed structures under the action of ion or neutron irradiation has not yet been studied. This issue is especially relevant for materials used under conditions of increased radiation loads, for example, in elements of spacecraft that are constantly exposed to cosmic radiation or in the structures of nuclear power plants.

The modified tungsten surface will undergo a high plasma flux in the fusion reactor. It is known that there will be no plasma interaction with the first wall material during the fusion device operation in the stationary mode. Plasma flow inconsistencies, such as edge-localized modes (ELMs), are the only reasons for such interaction [18,19]. However, the plasma parameters during the compression plasma flows treatment are close to those of plasma disruption in a fusion device [18,20]. As the modification of the tungsten surface occurs at the same parameters, the modified layer is assumed to be stable. Moreover, the stability of the surface under the plasma flux is determined mainly by the material's melting point. The small amount of extra elements, like copper and zirconium, will not change the melting point dramatically.

The interaction of a fusion reactor's first wall and divertor with helium plasma as a fusion product can lead to significant surface damage [21]. Neutron irradiation can also lead to transmutation reactions in the reactor's materials and helium bubble formation, which reduce the threshold stress for crack generation, and deteriorate tungsten's mechanical and physical characteristics [22]. W and Cu, Cu, and Zr alloys have been widely studied for use in fusion reactor components. Tungsten W is studied as a primary candidate for PFM for fusion reactors due to its mechanical properties, large thermal conductivity value (~173 $W \cdot m^{-1} \cdot K^{-1}$ at 293 K and 100 $W \cdot m^{-1} \cdot K^{-1}$ at 1273 K), and high resistance to sputtering [23]. But tungsten can experience radiation and heat-induced embrittlement [21]. Alloys of W and Cu could improve the ductility of W. Copper also has large thermal conductivity (~390 $W \cdot m^{-1} \cdot K^{-1}$ at 293 K) and its alloys such as CuCrZr were considered for removing heat from a divertor, for example, in cooling tubes, but Cu melts at a lower temperature than tungsten [23]. In W and Cu components, large stresses are assumed to

arise due to discrepancies between their thermal deformations, which can increase the fatigue of materials [23]. On the other hand, W-Cu composites were found to be still susceptible to radiation embrittlement during neutron irradiation, probably due to copper atoms' diffusion into W, which affected the flow of defects [9].

There were other studies that had previously sought whether plasma treatment can improve not only mechanical properties, but also radiation resistance. For example, it was shown that CrN coatings, which were deposited on W substrate using an arc ion plasma PVD technique, exfoliated after 1 MeV proton beam irradiation [7]. But it was also shown that after the first pulse of hydrogen plasma at 100 J/cm^2 at ELM-like conditions, the rate of tungsten surface erosion declined due to whole surface melting and smoothening [24].

Resistance of W to He ion irradiation was also studied widely. It was found that at low ion energies and room temperature, helium irradiation can produce bubbles by replacing interstitials [25]. Zhao et al. [26] showed that at a sufficiently large He ion fluence, helium bubbles start to form in W at a fluence of 3 $\times$ 10^{17} cm^{-2}. Research on Cu/W(Re) multilayered films showed that in samples irradiated by low-energy 60 keV He ions at a fluence of 2 $\times$ 10^{17} cm^{-2}, He bubbles tended to accumulate more in the Cu layer [27]. It was suggested that in a $W_{0.5}$ ZrC alloy, helium bubbles started appearing at higher damaging doses compared to pure W due to ZrC nanoparticles hindering He bubble growth at temperatures of 800–1000 °C [8]. This way, there appear to be few studies of the plasma treatment effect on the resistance to helium ion irradiation and blistering of tungsten and its alloys with Cu/Zr.

Thus, the purpose of this work was to study the behavior of the structural state of tungsten alloys modified by plasma action and irradiated with helium ions. The choice of tungsten alloys is due to their promising use in components of designed thermonuclear reactors.

2. Materials and Methods

For this study, the samples were pure polycrystalline tungsten plates with the dimensions of 10 mm $\times$ 10 mm $\times$ 2 mm. Two W samples were coated by a 2 μm thick layer of copper and zirconium separately by the arc vacuum technique.

Cu- and Zr-coated tungsten plates were subjected to compression plasma flow (CPF) impact in a magnetoplasma compressor. The compression plasma flows were produced by the equipment discussed in [28]. CPF is a type of gas-discharge plasma. The electrical discharge was produced in a special discharge device containing the central rod as a cathode and eight radial rods as anodes. The peak current during the discharge was about 70–100 kA during the discharge time 100 μs. Between the electrodes, the plasma state was generated and pushed out with a high velocity (50–100 km/s). The produced plasma stream was compressed by its own magnetic field and had a high concentration of charged particles (10^{17} cm^{-3}). In the discharge time interval, evaluated as 100 μs, the flow of compressed plasma retained stability, but it began to diverge when the time exceeded this interval.

The experiments were performed using the procedure described in [14]. In a "residual gas" mode, nitrogen gas at a pressure of 400 Pa filled a chamber, where a vacuum was obtained before filling. The samples were positioned vertically at a distance of 6 cm from the electrode edge. A constant voltage of 4.0 kV was applied between the electrodes. Such parameters allowed the production of a plasma stream with an absorbed energy density of 70 J/cm^2. The plasma stream's diameter when it reached the target was approximately 2–3 cm. The CPF influence on the samples was in the form of three pulses with an interval of 20–30 s.

The elemental composition, surface morphology, and phase composition of the W, W-Cu, and W-Zr alloys were analyzed after the CPF influence. The distribution of elements

of the coatings was measured by energy-dispersive X-ray spectroscopy (EDS) utilizing an Oxford MaxN analyzer (Oxford Instruments, Oxford, UK) in a Hitachi TM3030 scanning electron microscope (Hitachi, Tokyo, Japan). The surface morphology analysis was carried out by scanning electron microscopy (SEM) in a Hitachi TM3030 microscope at an accelerating voltage of 15 kV. Sizes of grains and cells were estimated using ImageJ software (version 1.54d) [29].

The phase contents of the surface of the tungsten samples were studied using the grazing incidence X-ray diffraction (GIXRD) method in an Ultima IV RIGAKU diffractometer (Rigaku, Tokyo, Japan) with CuKα radiation (λ = 0.154178 nm). The phase composition was measured at a grazing angle of 5°. The error in the lattice constant calculation with the XRD method was less than 0.1%. The method of $\sin^2\psi$ at a grazing incidence beam ($\alpha = 2.7^\circ$) was used to measure the residual stresses. The error of the stress measurement did not exceed 20%.

The irradiation of W, W-Cu, W-Zr samples was performed at a DC-60 cyclotron at the Astana branch of the Institute of Nuclear Physics (Kazakhstan) [30]. The targets were placed in a vacuum chamber designed for irradiating targets with low-energy ion beams. At the time of irradiation, the samples were attached to a water-cooled target holder to minimize the influence of thermal heating as a result of the accumulation of the irradiation dose. The irradiation experiment was performed under high vacuum conditions sustained at values of (1.3–6.7) $\times 10^{-3}$ Pa. Irradiation was carried out with He^{2+} ions with an energy of 40 keV at fluences of 1×10^{17} cm^{-2}, 2×10^{17} cm^{-2}, 3×10^{17} cm^{-2}.

3. Results and Discussion

The action of compression plasma flows with an energy density of 70 J/cm^2 on the tungsten samples and on the samples with pre-applied copper and zirconium coatings ensures heating of the near-surface layer above the melting point of tungsten. Consequently, melting of the applied copper and zirconium coatings also takes place. According to the calculations of the spatial temperature distribution after pulsed high-energy plasma action, based on taking into account only the effect of thermal conductivity [28], it was demonstrated that the depth of the molten layer is about 15 μm. The presence of thin copper or zirconium coatings on the surface, which have lower melting temperatures, has virtually no effect on the depth of the molten layer. A sufficiently high duration of the plasma flow pulse, amounting to 100 μs, increases the role of the liquid-phase process of melt mixing. The central mechanism of this process can be described in the following way. When the plasma flow reaches the surface of the material, there is intensive evaporation of atoms from the surface, which form the gas–plasma phase and localize near the surface, and the incident plasma flow prevents their dispersion in the chamber of the magnetoplasma compressor. This gas–plasma layer, called the shock-compressed layer, gradually increases its pressure due to the continuing evaporation of atoms from the surface of the target. The increase in pressure in the shock-compressed layer leads to its expansion, and the moving layers of this layer force the layers of the melt located directly on the surface to move. Due to the forces of viscous friction, the speed of spreading of the melt, which is directed mainly along the surface, spreads to the underlying layers. Thus, the movement of the molten layer is ensured. In the presence of a molten coating of another metal on the surface of tungsten, the hydrodynamic spreading of both metals allows them to mix due to the development of Kelvin–Helmholtz instability [31]. Viscous friction forces in the melt do not have time to cause the mixing to fade since after the plasma flow pulse duration ends, the heat supply ceases, and melt crystallization begins. The samples under study were 2 mm thick, much greater than the thickness of the molten layer, which ensures intensive heat removal to the volume of the unmelted part of the metal. According to theoretical estimates

made when solving the heat conductivity equation, the cooling rate is 10^6–10^7 K/s. Thus, within 10–20 μs after the end of the plasma pulse, the near-surface tungsten layer becomes completely crystallized, and within a few milliseconds, its temperature becomes equal to room temperature. As a result, a modified layer of a thickness equal to the melt depth is formed on the tungsten surface, and in the case of preliminary application of another metal coating, it contains atoms of this coating, representing an alloyed layer.

The samples' surface morphology and element distribution after exposure to compression plasma flows were studied using SEM and EDS analysis. According to the data (Figures 1 and 2), a visible grain structure with an average grain size of 2–3 μm can be found on the tungsten surface. The observed contrast of individual grains is due to the high reflectivity of tungsten atomic planes for incident electrons. Since each grain is turned by a certain crystallographic plane to the surface, the number of reflected electrons is also different. A cellular substructure can be found inside the grains due to the high-speed crystallization process, during which the flat crystallization front loses stability and takes a curved shape. The inhomogeneities that arise in this way on the crystallization front do not have time to disappear and develop throughout the entire solidification time. As a result, cells with an average size of 220–320 nm are formed on the surface. The observed cells have the same crystallographic orientation inside their own grain. In contrast to grain boundaries, the cells are limited by low-angle boundaries that are produced by dislocation aggregations.

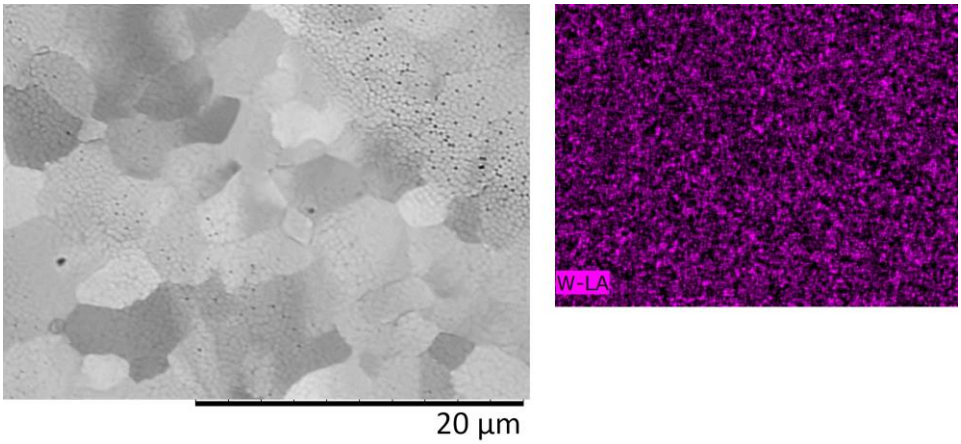

Figure 1. SEM image and EDS map of element distribution in W (CPF) sample.

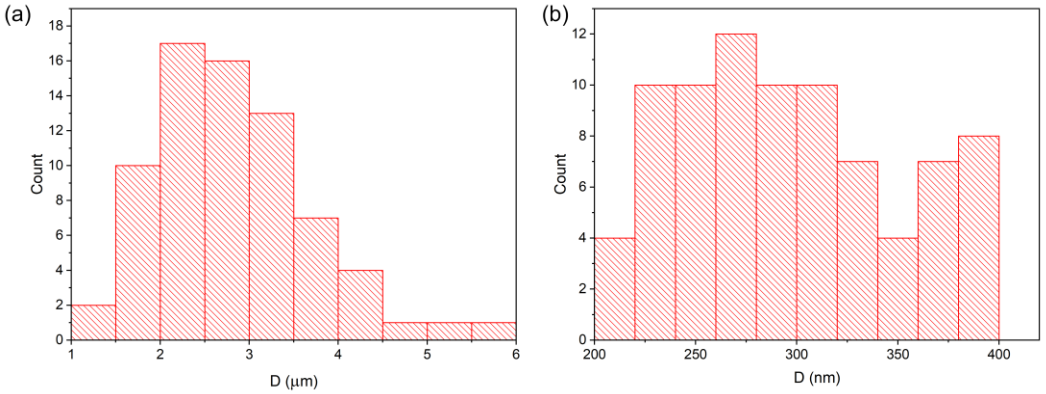

Figure 2. Sizes of (**a**) grains and (**b**) cells measured from the SEM image of W (CPF) sample in Figure 1.

In the case of the action of a compression plasma flow on tungsten with a pre-applied copper coating, it leads to the melting of both metals and the formation of a two-component

surface layer (Figure 3). However, a feature of the binary tungsten–copper system is the absolute immiscibility of components both in the liquid and solid states; the enthalpy of mixing of such a system always has a positive value [32]. This leads to the fact that in the molten state of two metals, their stratification into two phases occurs, which crystallize independently. Figure 3 shows a surface area with a clear boundary between the tungsten and copper phases, confirmed by EDS data. According to the EDS results, in the W-Cu samples treated with CPF, the concentration of W is 92.1 ± 2.8 atomic percents (at.%) and the Cu concentration is 7.9 ± 0.1 at. %. A system of surface cracks corresponding to tungsten can be seen on the surface area. Their formation occurs due to the action of thermoelastic stresses arising in the solid phase during rapid cooling. Indeed, since the liquid state has two separated phases, tungsten, having a higher melting point, begins to crystallize first, and high thermoelastic stresses arise there, leading to cracking. The cracks are observed mainly in the tungsten–copper alloys. During the crystallization of such systems, two separate phases are formed, which crystallize at different times (their lifetime is different). Copper and tungsten have different linear coefficients of thermal expansion. With complete crystallization of two phases (copper and tungsten), the amount of deformation at the interface on the copper side propagates into the region of solid tungsten. This is where cracks begin to spread, while the copper has higher plasticity and thermal deformation produces local plastic flow without surface cracking. In the pure tungsten and the tungsten–zirconium alloy modified with plasma exposure, predominant crystallization of a single-phase system occurs, which is characterized by a specific value of the coefficient of thermal expansion. The result of this is a uniform expansion of the entire near-surface layer and no cracks form.

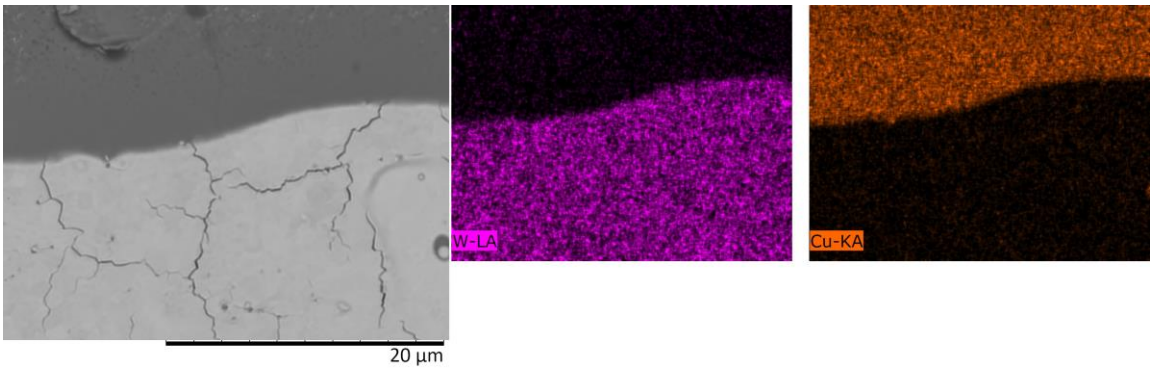

Figure 3. SEM image and EDS map of the element distribution in the W-Cu (CPF) sample.

The binary system tungsten–zirconium is characterized by miscibility in the liquid phase and limited miscibility in the solid phase. Therefore, after the action of a compression plasma flow on tungsten with a pre-applied zirconium coating, they mix in the melt, and a surface layer of tungsten alloyed with zirconium is formed (Figure 4). According to the EDS results, W-Zr treated with CPF contains W (66.4 ± 2.7 at.%) and Zr (33.6 ± 0.8 at.%). The analyzed layer consists of tungsten and zirconium atoms, proving their mixing in the melted state. As well as a pure tungsten surface, the surface of the tungsten–zirconium alloy exhibits a cellular structure.

The plasma-modified tungsten, tungsten–copper, and tungsten–zirconium alloy samples were irradiated with helium ions with an energy of 40 keV. Helium ion fluences ranged from 1×10^{17} to 3×10^{17} cm^{-2}. The results of modeling the ion ranges and radiation damage carried out in the Stopping and Range of Ions in Matter (SRIM) program [33] showed that the penetration depth of helium ions in the studied materials does not exceed 210 nm, and the maximum concentration distribution is at depths of around 90–120 nm. The calculation was performed in quick Kinchin–Pease mode and using the following

threshold displacement energies: 90 eV (W), 30 eV (Cu) [27], and 40 eV (Zr) [34]. Figure 5 shows that W, W-Cu, and W-Zr alloys have similar irradiation damage profiles with peaks in the range of 7–9 displacements-per-atom (dpa), and similar implanted helium profiles with peaks in the range of 24–30 atomic percents (at.%). The X-ray structural analysis in the geometry of the grazing beam was carried out to analyze the radiation damage of the modified layers.

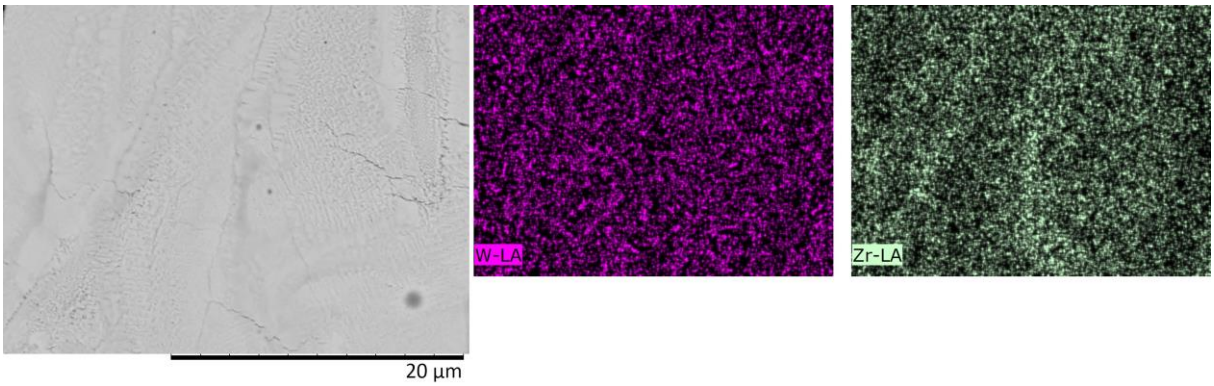

Figure 4. SEM image and EDS map of the element distribution in the W-Zr (CPF) sample.

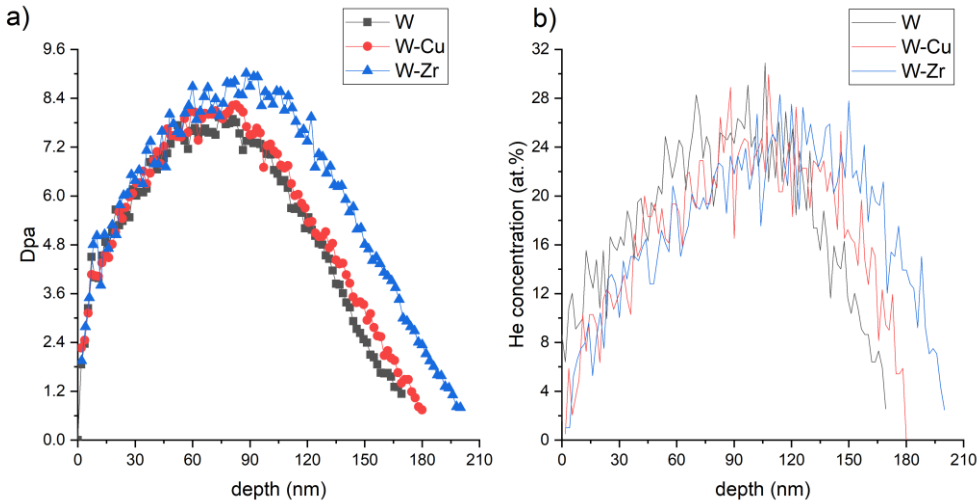

Figure 5. (**a**) Radiation damage (dpa) and (**b**) concentration of implanted helium atoms for W, W-Cu, W-Zr alloys calculated by SRIM for the irradiation by 40 keV He ions with a fluence of 3×10^{17} cm^{-2}.

Figure 6a shows the X-ray diffraction patterns of tungsten in its initial state, without plasma treatment, which was irradiated with helium ions. The analyzed layer has a polycrystalline structure with a predominant grain orientation (211), which does not change during ion irradiation. The goal was to obtain information from a layer of as small a thickness as possible, in which the main radiation defects are concentrated. It is known that X-ray diffraction analyzes a fairly thin layer and as the diffraction angle increases, the thickness of this layer increases. At small diffraction angles, the thickness of the analyzed layer is comparable to the implanted layer and the influence of the underlying layer can be minimized. For this reason, the first diffraction line (110) was chosen for investigation. However, a shoulder on the side of small diffraction angles can be seen on all diffraction lines of tungsten (Figure 6a, inset). The GIXRD method was implemented at an incidence angle of 5°, which made it possible to analyze a near-surface layer with a depth of about 1 µm. Thus, the obtained diffraction pattern is a superposition of the irradiated part of tungsten and that part of it is located below the irradiated layer, in which there are no radiation defects. Consequently, the appearance of a shoulder on the side of small

diffraction angles can be associated with forming a disordered tungsten phase W′ with a distorted crystal lattice. A similar phase is also detected during irradiation of tungsten preliminarily modified by plasma action (Figure 6b). However, in this case, the intensity of additional diffraction lines from the W′ phase is significantly lower than in tungsten without plasma treatment. It can be assumed that the implantation depth of helium ions does not depend on preliminary plasma treatment since it is determined mainly by the interaction with the target atoms. The main result of the plasma flow is a change in the grain and subgrain structure, which can affect the number of radiation defects. Consequently, a decrease in the proportion of the disordered W′ phase in modified tungsten can be due to a decrease in the number of defects (vacancies, interstitial atoms), the sinks for which are the grain and cell boundaries.

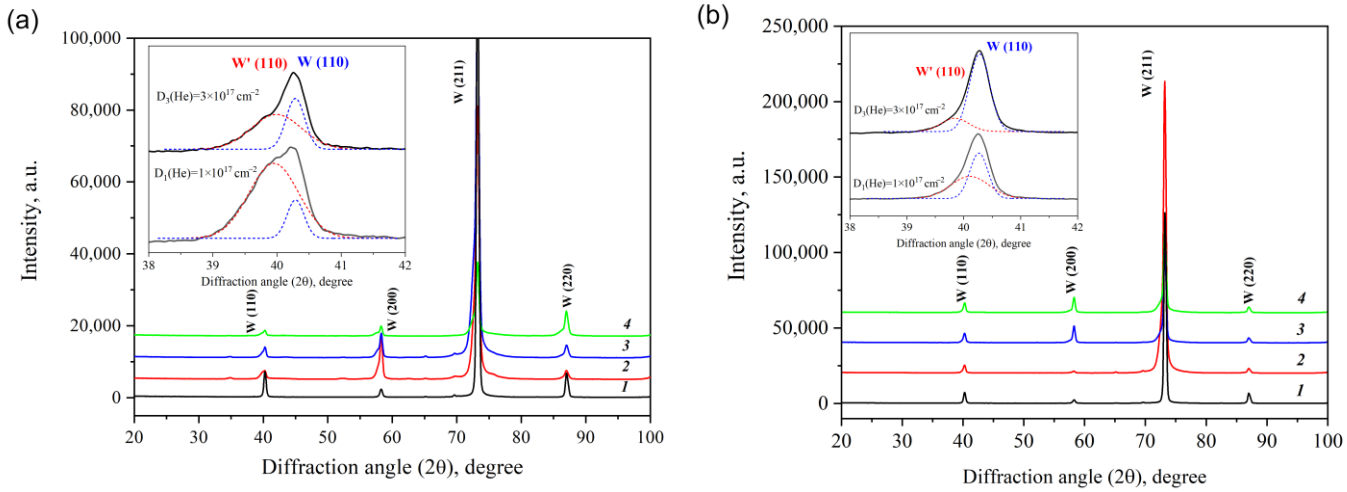

Figure 6. XRD patterns of (**a**) W (without plasma treatment) and (**b**) W after plasma treatment, both (1) before irradiation and after irradiation with He ions' fluences of (2) 1×10^{17} cm^{-2}, (3) 2×10^{17} cm^{-2}, and (4) 3×10^{17} cm^{-2}.

The W′ phase refers to the surface layer of tungsten, which contains a fairly large number of radiation defects that distort the crystal lattice. It is known that the distribution profile of implanted atoms (ions) is Gaussian. The distribution profile of defects, such as vacancies and interstitial atoms, practically coincides in depth and shape with the depth distribution profile of ions. However, at the ion energies used (40 keV), the depth of the implanted layer and the layer with radiation defects is about 200 nm, which is significantly less than the depth of the layer that is analyzed by X-ray diffraction. Therefore, two diffraction peaks appear in the diffraction spectra, one from the non-implanted part (W phase) and a peak from the implanted part (W′ phase). Since defects such as interstitial atoms and implanted ions appear in the crystal lattice during irradiation, they occupy positions in the interstitial sites and increase the lattice parameter.

The appearance of a disordered W′ phase was detected in tungsten alloyed with copper and zirconium (Figure 7a,b). However, in the zirconium-alloyed tungsten samples, the plasma-forming gas, nitrogen, interacts with zirconium, forming a thin layer of ZrN nitride on the surface. Tungsten and copper practically do not interact with nitrogen, so nitride phases were not observed in the previous systems. The appearance of zirconium nitride can be explained as follows. When the plasma flow interacts with the surface of a metal target, after the end of the plasma flow pulse, the shock-compressed layer is scattered, and the plasma-forming gas reaches the surface of the heated target. Due to solid-phase diffusion, it penetrates the crystallized layer with subsequent growth of a thin nitride layer on the surface. The appearance of a diffraction signal from ZrN was detected by X-ray

structural analysis (Figure 7b, inset). However, with an increase in the fluence of helium ions from 1×10^{17} to 3×10^{17} cm^{-2}, the diffraction maximum corresponding to the nitride phase disappears, which can be the result of both surface amorphization and sputtering by helium ions. However, elemental analysis did not find the nitrogen element on the surface after ion irradiation. Therefore, the total sputtering of the nitride layer with helium ions is a more probable result of the ion beam's influence.

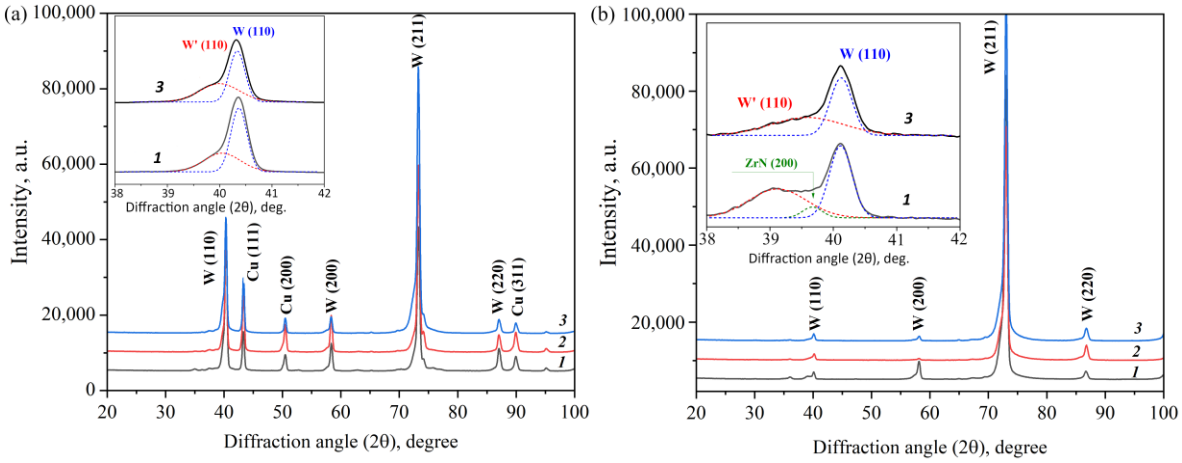

Figure 7. XRD patterns of (**a**) W-Cu alloy, (**b**) W-Zr alloy, both after irradiation with He ions at fluences of (1) 1×10^{17} cm^{-2}, (2) 2×10^{17} cm^{-2}, and (3) 3×10^{17} cm^{-2}.

Some weak diffraction peaks at the diffraction angles close to 35, 52, 65, and 70 degrees are observed on the XRD patterns of the treated samples. They are due to the appearance of small amounts of impurities during plasma treatment and ion irradiation. Most of them belong to oxide and carbide phases formed as thin native films on the surface; they do not affect the general patterns of phase changes during irradiation.

Localization of helium ions in the implanted layer and the generation of radiation defects leads to a change in the lattice parameters of the crystal structure. Table 1 presents the results of calculating the lattice parameter of the cubic unit cell of the body-centered cubic (bcc) tungsten phase (W) and the bcc phase of disordered tungsten (W') in the implanted layer. It can be seen that the W phase, which corresponds to a narrow diffraction maximum on the side of large diffraction angles, has a lattice parameter that is practically no different from the standard value, and these values do not depend on the ion irradiation dose. This is typical for all analyzed samples. However, higher values of the tungsten lattice parameter in copper- and zirconium-doped samples can be due to the formation of W(Cu) and W(Zr) solid solutions by the substitution type with a distorted crystal lattice after plasma exposure. Although the immiscibility of tungsten and copper was previously noted, it can nevertheless be expected that under conditions of rapid cooling of the melt, which ensures a nonequilibrium crystallization process, their insignificant dissolution is possible.

The dose of implanted ions increased at a constant ion energy and was directly proportional to the fluence of He ions; therefore, the maximum projection depth did not change at different implantation doses. However, increasing the fluence increased the number of implanted ions and the number of primary radiation defects. In the near-surface layer, transport of defects takes place, leading to an increase in the thickness of the layer containing the W' phase.

A higher lattice parameter characterizes the W' phase than the W phase. Indeed, this may result from the penetration of helium ions into the lattice and their dissolution. For all the analyzed systems, except for the W-Zr system, the lattice parameter of the W' phase increases with the dose of implanted helium ions. An inverse relationship is observed

for zirconium-doped tungsten: with an increase in the dose of implanted helium ions, the lattice parameter of the W′ phase decreases from 0.326 to 0.322 nm. A higher value of the lattice parameter at a small implantation dose can be explained by the presence of a zirconium nitride layer on the sample surface, the thickness of which is less than the projected range of helium ions. Penetrating through the ZrN nitride layer and reaching into the tungsten layer, helium ions form defects, among which there are vacancies. At the same time, radiation defects are also formed in the nitride layer, among which there are knocked-out zirconium atoms. The nitrogen atoms localized in the nitride layer are sputtered more effectively in comparison to zirconium atoms because of a big difference in masses. Therefore, the top layer of the W-Zr alloy becomes oversaturated with zirconium atoms. At the boundary between the nitride layer and tungsten, zirconium atoms penetrate the tungsten layer via the vacancy mechanism, thereby increasing its lattice parameter. When the dose of implanted helium ions increases to 3×10^{17} cm^{-2}, the nitride layer is completely sputtered, and mutual penetration of metal atoms does not occur; the lattice parameter of the W′ phase is determined only by the radiation defects introduced into it.

Table 1. Lattice parameter (nm) of the W and W′ phases after irradiation with helium ions.

Sample	W Phase		W′ Phase	
	$D_1 = 1 \times 10^{17}$ cm^{-2}	$D_3 = 3 \times 10^{17}$ cm^{-2}	$D_1 = 1 \times 10^{17}$ cm^{-2}	$D_3 = 3 \times 10^{17}$ cm^{-2}
a_0 (standard (JCPDS no. 004-0806))	0.3165 nm			
W (initial state)	0.317	0.317	0.319	0.319
W (after CPF)	0.317	0.317	0.318	0.320
W-Cu (after CPF)	0.316	0.316	0.318	0.319
W-Zr (after CPF)	0.318	0.318	0.326	0.322

The deformation of the tungsten crystal lattice caused by both plasma exposure and ion irradiation leads to residual internal stresses. The stresses were assessed by X-ray diffraction using the $\sin^2\Psi$ [35,36] method. XRD patterns were obtained in a grazing incidence geometry at an angle of 2.7° to the surface, which excluded the non-implanted layer of the samples and ensured a radiation penetration depth of 400–450 nm, corresponding to the implantation depth. The tungsten diffraction line (110) was used to calculate the internal stresses. A series of measurements of the interplanar distance d_Ψ were carried out at different angles Ψ between the diffraction angle and the normal to the sample surface, which made it possible to calculate the internal stresses using the following relationship:

$$d_\Psi = \left[\frac{1+\nu}{E} sin^2\Psi - \frac{2\nu}{E}\right]\sigma d_0 + d_0, \quad (1)$$

where ν is the Poisson's ratio of tungsten (0.28), E is the Young's modulus of tungsten (400 GPa), d_0 is the interplanar distance in an ideal crystal lattice, and σ is the stress value. Having linearized Equation (1) in the form $Y = aX$:

$$X = \frac{1+\nu}{E} sin^2\Psi - \frac{2\nu}{E}, Y = d_\Psi \quad (2)$$

the value of σ was found from the graphical method. Young's modulus E can be taken for pure tungsten in the case of the samples after plasma treatment and for the W-Cu systems due to the immiscibility of the components. In the W-Zr, we need to consider the change in the elastic parameters. The results of the stress estimation (with the elastic parameters for pure tungsten) are presented in Table 2.

Table 2. Stress values (GPa) in tungsten samples after plasma exposure and ion irradiation.

Sample	$D_1 = 1 \times 10^{17}$ cm^{-2}	$D_3 = 3 \times 10^{17}$ cm^{-2}
W (initial state)	0.10 ± 0.02	0.10 ± 0.02
W (after CPF)	0.90 ± 0.18	1.00 ± 0.20
W-Cu (after CPF)	1.20 ± 0.24	0.90 ± 0.18
W-Zr (after CPF)	0.60 ± 0.12	0.20 ± 0.04

According to the obtained data, the value of internal stress in the initial tungsten sample, which was not processed by the plasma flow, is 0.1 GPa and does not depend on the dose of implanted helium ions. The positive sign of the stresses indicates their stretching nature, apparently caused by implanted helium ions stretching the crystal lattice. Indeed, with an increase in the dose of implanted helium ions, their number in the near-surface layer should increase and lead to a growth in stresses. However, such an effect is not observed. This can be associated with a change in the surface morphology, on which traces of surface destruction can be seen. Increasing the dose of implanted ions ensures the relaxation of internal stresses due to local destruction of the tungsten surface (Figure 8).

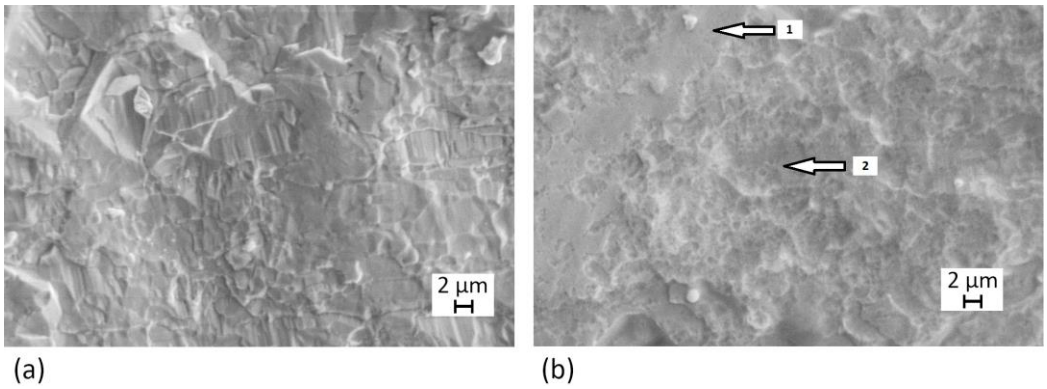

Figure 8. SEM images of the tungsten surface (without plasma treatment) after irradiation with He ions at fluences of (**a**) 1×10^{17} cm^{-2} and (**b**) 3×10^{17} cm^{-2} (1 is the area without ion sputtering, 2 is the area after ion sputtering).

In the plasma flow-modified tungsten samples, internal stresses increase slightly from 0.9 to 1.0 GPa with an increase in the dose of implanted helium ions from 1×10^{17} to 3×10^{17} cm^{-2}. A higher stress level compared to unmodified tungsten may be due to a fine-cell structure (Figure 1), in which the boundaries between the cells create additional stresses in the structure associated with excess surface energy. However, a higher stress level in modified tungsten does not lead to surface destruction (Figure 9). It results from cell structure refinement after high-speed crystallization of the tungsten surface layer. The dislocation aggregations on the boundaries block the plastic deformation and the strengthening effect occurs.

In the copper-doped tungsten samples, the maximum level of residual stresses of 0.9–1.2 GPa is achieved, which is associated not only with the refinement of the grain structure during high-speed crystallization but also with the presence of interphase boundaries between individual sections of tungsten and copper, which, due to the difference in elastic constants and thermal expansion coefficients, create additional stresses in each of the phases. Figure 10 shows the surface of the W-Cu alloy, treated by CPF and irradiated by helium ions, where darker areas represent Cu and lighter areas represent W. On the surface of the implanted samples, formed blisters are observed, which are localized exclusively in the areas of the tungsten phase (Figure 10). These blisters, containing clusters of helium

ions inside, can also create additional pressure on the crystal lattice of the surrounding phase, thereby increasing internal stresses.

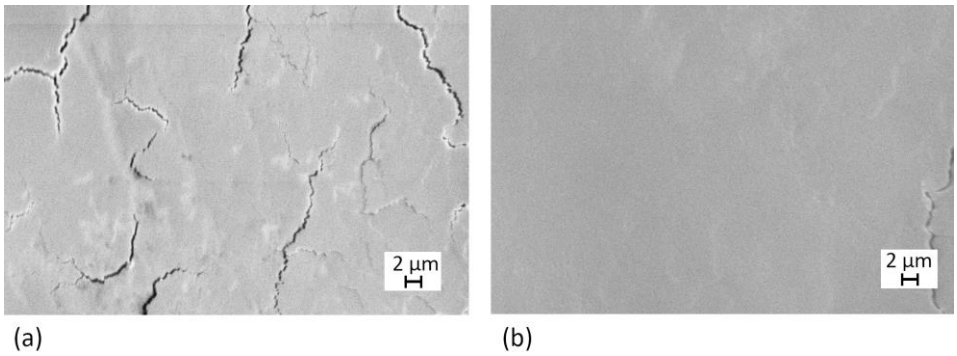

Figure 9. SEM images of the tungsten surface after plasma treatment and irradiation with He ions at fluences of (**a**) 1×10^{17} cm^{-2} and (**b**) 3×10^{17} cm^{-2} [37].

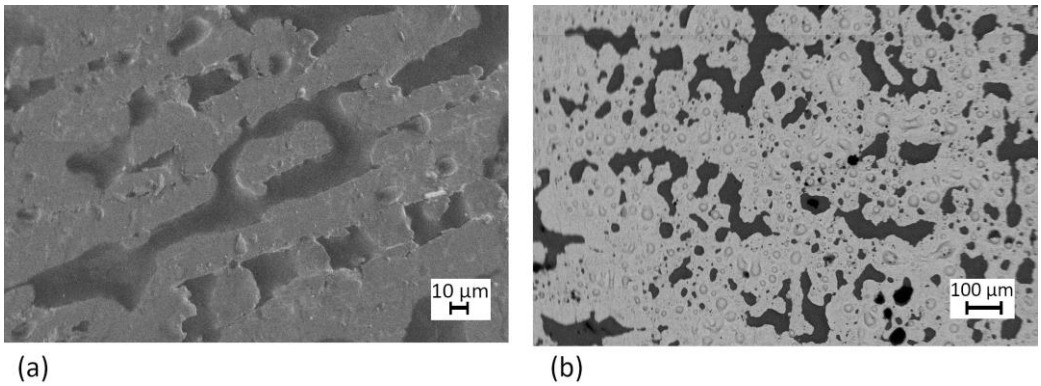

Figure 10. SEM images of the tungsten–copper alloy surface after plasma treatment and irradiation with He ions at fluences of (**a**) 1×10^{17} cm^{-2} and (**b**) 3×10^{17} cm^{-2}.

As is known, the formation of blisters on the surface is associated, first of all, with the accumulation of implanted helium ions in the near-surface region. In the pure tungsten treated with plasma, the high density of boundaries between cells is expected to accelerate the diffusive transport of implanted ions, which prevents their aggregation. In the W-Cu alloy, both phases are immiscible, and there is an interphase boundary between them. At this boundary, interfacial internal elastic stresses arise, which propagate in the tungsten crystal lattice. It is these stresses that prevent the transport of helium ions and lead to its accumulation in blisters.

The level of residual internal stresses in tungsten doped with zirconium atoms is 0.2–0.6 GPa. A decrease in the stress level in such a system is associated with a surface layer of zirconium nitride, which partially screens the effect of radiation defects on the tungsten structure. Scanning electron microscopy detected no surface damage in the tungsten–zirconium system (Figure 11).

In general, the results can be summarized as follows. Irradiation of tungsten with helium ions with an energy of 40 keV leads to the accumulation of implanted ions and primary radiation defects in a thin surface layer several hundred nanometers thick. The result of their accumulation is the deformation of the crystal lattice, which is designated as the W′ phase. In the case of preliminary plasma treatment, which involves melting the surface layer and its rapid crystallization, the surface layer is characterized by a dispersed cellular structure with an increased dislocation density at the cell boundaries. These dislocations create an increased field of elastic lattice distortions, which affect the migration of implanted helium ions and primary radiation defects. In this case, the layer thickness,

or volume fraction, of the tungsten layer with a distorted crystal lattice, the W′ phase, decreases. Reducing the thickness of the distorted layer makes it possible to reduce the level of internal stresses that cause surface destruction, leading to an increase in the radiation resistance of tungsten. Plasma treatment of tungsten can be carried out with the additional introduction of alloying elements such as copper or zirconium. The addition of copper to the surface layer of tungsten promotes the formation of a two-phase system due to their immiscibility with each other in both the liquid and solid states. Alloying tungsten with zirconium leads to the formation of a substitutional solid solution.

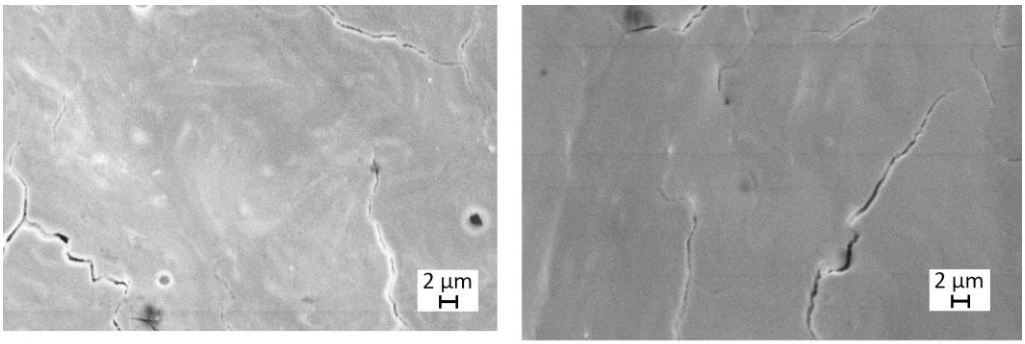

Figure 11. SEM images of the tungsten–zirconium surface after plasma treatment and irradiation with He ions at fluences of (**a**) 1×10^{17} cm^{-2} and (**b**) 3×10^{17} cm^{-2}.

4. Conclusions

This paper studies the effect of preliminary plasma treatment on radiation defects occurring in tungsten after irradiation with helium ions with an energy of 40 keV and doses of 1×10^{17}–3×10^{17} cm^{-2}. Exposure of tungsten to compression plasma flows with an energy density of 70 J/cm^2 allows modifying the grain structure of the surface layer, which becomes dispersed with an average cell size of 220–320 nm due to high-speed crystallization of the melt. Preliminary application of copper or zirconium coatings leads to alloying the tungsten layer with the applied elements due to liquid-phase mixing of the melt and subsequent high-speed crystallization.

Irradiation of modified samples with helium ions creates a structure in the thin surface layer based on the W′ phase with a bcc structure but with an increased lattice parameter value. Radiation defects arising in the near-surface layer contribute to forming internal residual tensile stresses, which reach 1.2 GPa. It was found that preliminary plasma flow treatment, creating a dispersed cellular structure, allows increasing the number of sinks for radiation defects, which are intergranular and interphase boundaries. As a result, the surface of tungsten samples without preliminary plasma treatment is destroyed with an increased dose of implanted helium ions due to the relaxation of internal stresses. Preliminary plasma flow treatment of tungsten, causing the formation of the layers with a dispersed cellular structure, a combination of two immiscible phases (in W-Cu alloy) and solid solution formation (in W-Zr alloy), leads to an increase in the radiation resistance of the surface layer. From a practical point of view, the preliminary plasma treatment of the tungsten surface allows for an increase in the radiation resistance of the top surface layer under helium ion irradiation.

Author Contributions: Conceptualization, V.U.; funding acquisition, A.R.; investigation, A.R., V.S., B.A., I.I., V.U., V.A., M.K., A.K. (Anton Kuzmitski) and A.K. (Alisher Kurakhmedov); methodology, A.R., V.S., V.U., V.A. and A.K. (Anton Kuzmitski); project administration, A.R. and V.U.; resources, A.R., V.S., I.I., V.U., V.A. and A.K. (Anton Kuzmitski); supervision, A.R., V.S. and V.U.; validation, A.R., V.S. and V.U.; visualization, A.R., V.S., B.A. and V.U.; writing—original draft, A.R., V.S., B.A.,

I.I., V.U., V.A., M.K., A.K. (Anton Kuzmitski) and A.K. (Alisher Kurakhmedov); writing—review and editing, A.R., V.S., B.A. and V.U. All authors have read and agreed to the published version of the manuscript.

Funding: This research was funded by the Science Committee of the Ministry of Science and Higher Education of the Republic of Kazakhstan (Grant No. AP14872078).

Institutional Review Board Statement: Not applicable.

Informed Consent Statement: Not applicable.

Data Availability Statement: The original contributions presented in this study are included in the article. Further inquiries can be directed to the corresponding authors.

Conflicts of Interest: The authors declare no conflicts of interest. The funders had no role in the design of the study; in the collection, analyses, or interpretation of data; in the writing of the manuscript; or in the decision to publish the results.

Abbreviations

The following abbreviations are used in this manuscript:

CPF	Compression plasma flows
EDS	Energy-dispersive X-ray spectroscopy
GIXRD	Grazing incidence X-ray diffraction
SEM	Scanning electron microscopy

References

1. Kikuchi, S.; Saiki, S.; Ohashi, T.; Nakazawa, K. Surface Modification for Steel Rods Based on Atmospheric-Pressure Nitrogen Plasma Treatment at Room Temperature. *Results Mater.* **2024**, *23*, 100612. [CrossRef]
2. Xia, T.; Yan, J.; Han, W.; Wang, Z.; Jiang, Z.; Wu, J.; Shi, Y.; Wang, Z.; Ye, X.; Wu, J.; et al. Surface Modification and Deuterium Retention in Rhenium Doped Tungsten Exposed to Low Energy Deuterium Plasma. *Fusion Eng. Des.* **2021**, *173*, 112936. [CrossRef]
3. Zheng, W.; Hu, M.; Zhou, Z.; Huang, M.; Feng, D.; Ma, Y.; Ren, S.; Yang, J. Microstructure Evolution and Fatigue Crack Propagation of AlCoCrFeNi2.1 High Entropy Alloy after Electron Beam Surface Modification. *Mater. Sci. Eng. A* **2024**, *913*, 147025. [CrossRef]
4. Zhao, G.; Zhang, P.; Li, J.; Zhang, Z.; Li, H.; Ma, L. Effects of Different Scanning Speeds on Microstructure Evolution and Tribological Properties of Inconel 718 Alloy Vacuum Electron Beam Surface Modification. *Mater. Today Sustain.* **2024**, *25*, 100613. [CrossRef]
5. Pariona, M.M.; Teleginski, V.; Santos, K.D.; Machado, S.; Zara, A.J.; Zurba, N.K.; Riva, R. Yb-Fiber Laser Beam Effects on the Surface Modification of Al–Fe Aerospace Alloy Obtaining Weld Filet Structures, Low Fine Porosity and Corrosion Resistance. *Surf. Coat. Technol.* **2012**, *206*, 2293–2301. [CrossRef]
6. Smayev, M.P.; Smirnov, P.A.; Budagovsky, I.A.; Fedyanina, M.E.; Glukhenkaya, V.B.; Romashkin, A.V.; Lazarenko, P.I.; Kozyukhin, S.A. Cylindrical Laser Beams for A-Ge2Sb2Te5 Thin Film Modification. *J. Non-Cryst. Solids* **2024**, *633*, 122952. [CrossRef]
7. Kawai, M.; Kokawa, H.; Michiuchi, M.; Kurisihita, H.; Goto, T.; Futakawa, M.; Yoshiie, T.; Hasegawa, A.; Watanabe, S.; Yamamura, T.; et al. Present Status of Study on Development of Materials Resistant to Radiation and Beam Impact. *J. Nucl. Mater.* **2008**, *377*, 21–27. [CrossRef]
8. Ipatova, I.; Greaves, G.; Terentyev, D.; Gilbert, M.R.; Chiu, Y.-L. TEM Investigation of Helium Bubble Evolution in Tungsten and ZrC-Strengthened Tungsten at 800 and 1000 °C under 40keV He+ Irradiation. *Nucl. Eng. Technol.* **2024**, *56*, 1490–1500. [CrossRef]
9. Zinovev, A.; Terentyev, D.; Chang, C.-C.; Yin, C.; Bakaev, A.; Rieth, M.; Lied, P.; Reiser, J.; Bonnekoh, C. Effect of Neutron Irradiation on Ductility of Tungsten Foils Developed for Tungsten-Copper Laminates. *Nucl. Mater. Energy* **2022**, *30*, 101133. [CrossRef]
10. Rotshtein, V.P.; Ivanov, Y.F.; Markov, A.B.; Proskurovsky, D.I.; Karlik, K.V.; Oskomov, K.V.; Uglov, B.V.; Kuleshov, A.K.; Novitskaya, M.V.; Dub, S.N.; et al. Surface Alloying of Stainless Steel 316 with Copper Using Pulsed Electron-Beam Melting of Film–Substrate System. *Surf. Coat. Technol.* **2006**, *200*, 6378–6383. [CrossRef]
11. Yeo, S. Properties of Fe2O3 Coating on Polymer Substrate by Ion Beam Mixing. *Int. J. Adhes. Adhes.* **2013**, *40*, 145–148. [CrossRef]
12. Piątkowska, A.; Jagielski, J.; Gawlik, G.; Matz, W.; Richter, E.; Mozetic, M.; Zalar, A. Study of Micromechanical Properties of Ion-Beam Mixed Tungsten-on-Steel Layers. *Wear* **2003**, *254*, 1037–1041. [CrossRef]

13. Surzhikov, A.P.; Frangulyan, T.S.; Ghyngazov, S.A.; Koval, N.N. Structural-Phase Transformations in near-Surface Layers of Alumina–Zirconium Ceramics Induced by Low-Energy High-Current Electron Beams. *Nucl. Instrum. Methods Phys. Res. Sect. B Beam Interact. Mater. At.* **2009**, *267*, 1072–1076. [CrossRef]
14. Ryskulov, A.; Shymanski, V.; Uglov, V.; Ivanov, I.; Astashynski, V.; Amanzhulov, B.; Kuzmitski, A.; Kurakhmedov, A.; Filipp, A.; Ungarbayev, Y.; et al. Structure and Phase Composition of WNb Alloy Formed by the Impact of Compression Plasma Flows. *Materials* **2023**, *16*, 4445. [CrossRef]
15. Shymanski, V.I.; Cherenda, N.N.; Uglov, V.V.; Astashynski, V.M.; Kuzmitski, A.M. Structure and Phase Composition of Nb/Ti System Subjected to Compression Plasma Flow Impact. *Surf. Coat. Technol.* **2015**, *278*, 183–189. [CrossRef]
16. Shymanski, V.I.; Jevdokimovs, A.; Cherenda, N.N.; Astashynski, V.M.; Petrikova, E.A. Structure and phase composition of hypereutectic silumin alloy Al–20Si after compression plasma flows impact. *J. Belarusian State Univ. Phys.* **2021**, *2*, 25–33. [CrossRef]
17. Cherenda, N.N.; Uglov, V.V.; Martinovich, Y.V.; Betanov, I.A.; Astashynski, V.M.; Kuzmitski, A.M. Structure of the austenitic steel surface layer subjected to compression plasma flows impact. *High Temp. Mater. Process.* **2020**, *24*, 211–225. [CrossRef]
18. Makhlai, V.A.; Garkusha, I.E.; Linke, J.; Malykhin, S.V.; Aksenov, N.N.; Byrka, O.V.; Herashchenko, S.S.; Surovitskiy, S.V.; Wirtz, M. Damaging of Tungsten and Tungsten–Tantalum Alloy Exposed in ITER ELM-like Conditions. *Nucl. Mater. Energy* **2016**, *9*, 116–122. [CrossRef]
19. Becoulet, M.; Huysmans, G.; Thomas, P.; Joffrin, E.; Rimini, F.; Monier-Garbet, P.; Grosman, A.; Ghendrih, P.; Parail, V.; Lomas, P.; et al. Edge Localized Modes Control: Experiment and Theory. *J. Nucl. Mater.* **2005**, *337–339*, 677–683. [CrossRef]
20. Klimov, N.S.; Podkovyrov, V.L.; Zhitlukhin, A.M.; Muzichenko, A.D.; Kovalenko, D.V.; Putrik, A.B.; Kupriyanov, I.B.; Giniyatulin, R.N.; Gervash, A.A.; Safronov, V.M. Plasma-Facing Materials Erosion under ITER-Like Transient Loads at QSPA Plasma Gun Facility. *Fusion Sci. Technol.* **2014**, *66*, 118–124. [CrossRef]
21. Zinkle, S.J.; Snead, L.L. Designing Radiation Resistance in Materials for Fusion Energy. *Annu. Rev. Mater. Res.* **2014**, *44*, 241–267. [CrossRef]
22. Rieth, M.; Doerner, R.; Hasegawa, A.; Ueda, Y.; Wirtz, M. Behavior of Tungsten under Irradiation and Plasma Interaction. *J. Nucl. Mater.* **2019**, *519*, 334–368. [CrossRef]
23. Ueda, Y.; Schmid, K.; Balden, M.; Coenen, J.W.; Loewenhoff, T.; Ito, A.; Hasegawa, A.; Hardie, C.; Porton, M.; Gilbert, M. Baseline High Heat Flux and Plasma Facing Materials for Fusion. *Nucl. Fusion* **2017**, *57*, 092006. [CrossRef]
24. Klimov, N.; Podkovyrov, V.; Zhitlukhin, A.; Kovalenko, D.; Bazylev, B.; Janeschitz, G.; Landman, I.; Pestchanyi, S.; Federici, G.; Loarte, A.; et al. Experimental Study of PFCs Erosion under ITER-like Transient Loads at Plasma Gun Facility QSPA. *J. Nucl. Mater.* **2009**, *390–391*, 721–726. [CrossRef]
25. Iwakiri, H.; Yasunaga, K.; Morishita, K.; Yoshida, N. Microstructure Evolution in Tungsten during Low-Energy Helium Ion Irradiation. *J. Nucl. Mater.* **2000**, *283–287*, 1134–1138. [CrossRef]
26. Zhao, M.; Liu, F.; Yang, Z.; Xu, Q.; Ding, F.; Li, X.; Zhou, H.; Luo, G.-N. Fluence Dependence of Helium Ion Irradiation Effects on the Microstructure and Mechanical Properties of Tungsten. *Nucl. Instrum. Methods Phys. Res. Sect. B Beam Interact. Mater. At.* **2018**, *414*, 121–125. [CrossRef]
27. Pu, G.; Sun, H.; Wang, Y.; Li, J.; Du, X.; Liu, B.; Ren, D.; Zhang, K.; Li, G.; Lin, L. Effect of Periodic Thickness on the Helium Bubble Evolution and Irradiation Hardening in Cu/W(Re) Multi-Layered Films under Helium Ion Irradiation. *J. Alloys Compd.* **2023**, *935*, 167978. [CrossRef]
28. Shymanski, V.I.; Uglov, V.V.; Cherenda, N.N.; Pigasova, V.S.; Astashynski, V.M.; Kuzmitski, A.M.; Zhong, H.W.; Zhang, S.J.; Le, X.Y.; Remnev, G.E. Structure and Phase Composition of Tungsten Alloys Modified by Compression Plasma Flows and High-Intense Pulsed Ion Beam Impacts. *Appl. Surf. Sci.* **2019**, *491*, 43–52. [CrossRef]
29. Schneider, C.A.; Rasband, W.S.; Eliceiri, K.W. NIH Image to ImageJ: 25 Years of Image Analysis. *Nat. Methods* **2012**, *9*, 671–675. [CrossRef] [PubMed]
30. Zdorovets, M.; Ivanov, I.; Koloberdin, M.; Kozin, S.; Alexandrenko, V.; Sambaev, E.; Kurakhmedov, A.; Ryskulov, A. Accelerator Complex Based on DC-60 Cyclotron. In Proceedings of the XXIV Russian Particle Accelerator Conference RUPAC 2014, Obninsk, Russia, 6–10 October 2014; Joint Accelerator Conferences Website (JACoW): Geneva, Switzerland, 2014; pp. 287–289.
31. Asthana, R.; Agrawal, G.S. Viscous Potential Flow Analysis of Electrohydrodynamic Kelvin–Helmholtz Instability with Heat and Mass Transfer. *Int. J. Eng. Sci.* **2010**, *48*, 1925–1936. [CrossRef]
32. Ma, E. Alloys Created between Immiscible Elements. *Prog. Mater. Sci.* **2005**, *50*, 413–509. [CrossRef]
33. Ziegler, J.F.; Ziegler, M.D.; Biersack, J.P. SRIM—The Stopping and Range of Ions in Matter (2010). *Nucl. Instrum. Methods Phys. Res. Sect. B Beam Interact. Mater. At.* **2010**, *268*, 1818–1823. [CrossRef]
34. Was, G.S. *Fundamentals of Radiation Materials Science: Metals and Alloys*; Springer: Berlin/Heidelberg, Germany; New York, NY, USA, 2007; ISBN 978-3-540-49471-3.
35. Luo, Q.; Jones, A.H. High-Precision Determination of Residual Stress of Polycrystalline Coatings Using Optimised XRD-Sin2ψ Technique. *Surf. Coat. Technol.* **2010**, *205*, 1403–1408. [CrossRef]

36. Haase, A.; Klatt, M.; Schafmeister, A.; Stabenow, R.; Ortner, B. The Generalized Sin2 ψ Method: An Advanced Solution for X-Ray Stress Analysis in Textured Materials. *Powder Diffr.* **2014**, *29*, 133–136. [CrossRef]
37. Ryskulov, A.; Shymanski, V.; Ivanov, I.; Amanzhulov, B.; Dauhaliuk, A.; Uglov, V.; Temir, A.; Astashynski, V.; Sapar, A.; Kuzmitski, A.; et al. Radiation Effects in Tungsten and Tungsten-Copper Alloys Treated with Compression Plasma Flows and Irradiated with He Ions. *Mater.* **2024**, *17*, 4442. [CrossRef] [PubMed]